UC Riverside

UC Riverside Previously Published Works

Title

Nonthermal Plasma Activation of Adsorbates: The Case of CO on Pt

Permalink

https://escholarship.org/uc/item/79q6q1m5

Journal

JACS Au, 4(8)

ISSN

2691-3704

Authors

Kim, Minseok
Biswas, Sohag
Alvarez, Isabel Barraza
et al.

Publication Date

2024-08-26

DOI

10.1021/jacsau.4c00309

Copyright Information

This work is made available under the terms of a Creative Commons Attribution-NonCommercial-NoDerivatives License, available at https://creativecommons.org/licenses/by-nc-nd/4.0/

Peer reviewed

eScholarship.org Powered by the California Digital Library
University of California

JACS Au
AN OPEN ACCESS JOURNAL OF THE AMERICAN CHEMICAL SOCIETY

Open Access
This article is licensed under CC-BY-NC-ND 4.0

pubs.acs.org/jacsau
Article

Nonthermal Plasma Activation of Adsorbates: The Case of CO on Pt

Minseok Kim, Sohag Biswas, Isabel Barraza Alvarez, Phillip Christopher,* Bryan M. Wong,* and Lorenzo Mangolini*

Cite This: JACS Au 2024, 4, 2979−2988
Read Online

ACCESS | Metrics & More | Article Recommendations | Supporting Information

ABSTRACT: Nonthermal plasmas provide a unique approach to electrically driven heterogeneous catalytic processes. Despite much interest from the community, fundamental activation pathways in these processes remain poorly understood. Here, we investigate how exposure to a nonthermal plasma sustained in an argon nonreactive atmosphere affects the desorption of carbon monoxide (CO) from platinum nanoparticles. Temperature-programmed desorption measurements indicate that the plasma reduces the effective binding energy (BE) of CO to Pt surfaces by as much as ∼0.3 eV, with the reduction in the BE scaling linearly with the plasma density. We find that the effective CO BE is most strongly reduced for under-coordinated sites (steps and edges) compared to well-coordinated sites (terraces). Density functional theory calculations suggest that this is due to plasma-induced charging and electric fields at the catalyst surface, which preferentially affect under-coordinated sites. This study provides direct experimental evidence of plasma-induced nonthermal activation of the adsorbate-catalyst couple.

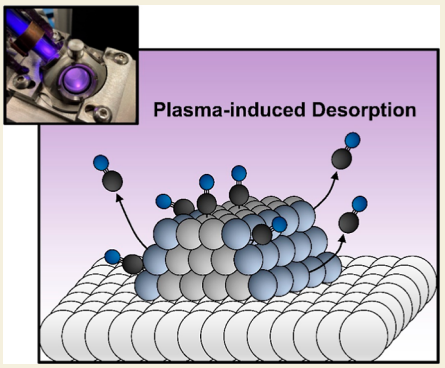

KEYWORDS: *nonthermal plasma, carbon monoxide, platinum, binding energy, DFT calculations, surface charging*

INTRODUCTION

There is a societal need for novel approaches to heterogeneous catalysis that can mitigate, or eliminate, the environmental concerns associated with thermally driven processes.[1−3] Among the proposed solutions, nonthermal plasma-induced catalysis, when combined with renewable energy resources, has the potential to reduce anthropogenic greenhouse gas emissions.[4−7] The most important characteristic of a nonthermal plasma is its intrinsic nonequilibrium state between energetic electrons and other species, such as ions and neutral molecules. This property allows for the activation of highly stable molecules such as CO_2, CH_4, and N_2 at room temperature in addition to the potential for bond-specific chemistry.[8] As a consequence, reports are abundant in the literature about the combination of nonthermal plasmas with heterogeneous catalysts. Examples include CO_2 conversion,[9] production of NH_3[10,11] and NO_X,[12] as well as CH_4 reforming.[13] Considerable effort has been dedicated to assessing the reactor-level yield, selectivity, and energy cost associated with nonthermal plasma-driven catalysis.[14−16] Unfortunately, the microscopic-level reaction pathways in these complex systems remain poorly understood, inevitably hampering the further development of these exciting processes.

The plasma community has made widespread use of microkinetic models to gain insights into molecular activation and reaction pathways in nonthermal plasma catalysis.[17,18] Such models often utilize modified rates of dissociative adsorption that attempt to account for the gas-phase activation of the reactant molecules. Vibrational excitation or dissociation of molecular nitrogen in plasmas has been used to justify its fixation at room temperature.[12,19] Similarly, vibrational excitation of methane or CO_2 has been proposed as the critical activation mechanism in these systems.[20,21] While the activation of molecules in the gas phase is likely to play a role, other activation pathways may be present as well.

On the experimental side, the community has also made extensive use of in situ characterization tools to identify reaction pathways at the plasma−catalyst interface.[21,22] For instance, Kim et al. use transmission infrared spectroscopy and find that CO conversion to CO_2 is facilitated on ZnO surfaces because of plasma-induced CO vibrational excitation.[23] Xu et al. use in situ Fourier-transform infrared spectroscopy (FTIR) to identify reaction intermediates during the plasma-induced hydrogenation of CO_2 on Ru catalysts and find them to be completely different than that for the case of a thermally driven reaction.[24] While powerful, the majority of research groups use dielectric barrier discharges (DBDs) for their study. This configuration inevitably generates a strongly nonuniform, transient plasma, making it difficult to isolate activation pathways on catalyst surfaces.

Received: April 4, 2024
Revised: June 7, 2024
Accepted: July 5, 2024
Published: July 12, 2024

© 2024 The Authors. Published by American Chemical Society

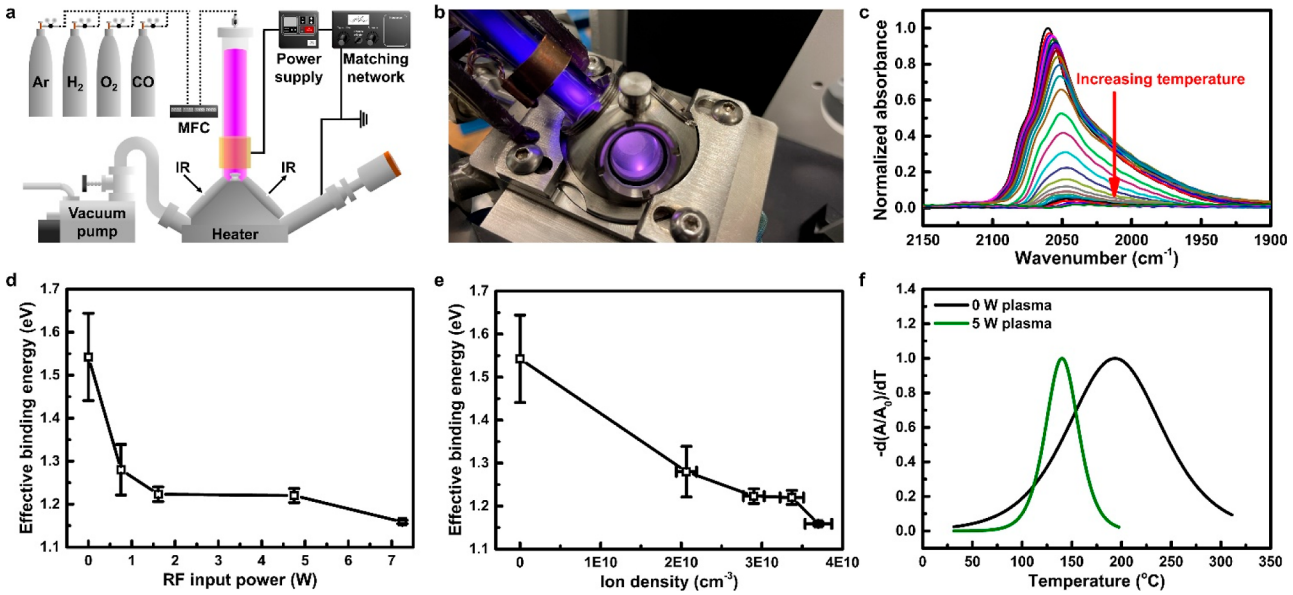

Figure 1. TPD using DRIFTS to measure the BE between CO and Pt with plasma exposure. (a) Schematic of the DRIFTS system coupled with an RF plasma reactor. (b) Photograph of the Ar plasma while in operation. (c) DRIFTS spectra during a TPD experiment at 1 min intervals as temperature increases. (d) Effective BE between CO and Pt as a function of the measured RF input power and (e) as a function of the measured ion density. Measurements for both effective BE and ion density were repeated three times to determine error bars. Effective BE shows near-linear dependence on the ion density and significantly decreases by ~0.3 eV at a plasma power of 1.6 W. (f) Normalized negative derivative of A/A_0 (A_0 being the normalized area at 30 °C) with respect to temperature. A broad peak without plasma implies that the desorption of CO is dependent on the coverage. The peak with the plasma shifts to a lower temperature and becomes narrower.

To further complicate things, nonthermal plasmas generate a complex nonequilibrium environment that can initiate surface reactions according to multiple competing pathways. Plasma exposure leads to a flux of multiple species toward exposed surfaces, including ions, electrons, excited species, and photons. For instance, a significant fraction of the power used to sustain a plasma results in the generation of photons with complex energy spectra. The formation of an electrical double-layer, or sheath, at plasma-exposed surfaces is an intrinsic aspect of these nonequilibrium discharges. This results in both surface charging and the acceleration of ions toward the surface. These mechanisms proceed in parallel and can affect the surface reaction rates. Zhang et al. found that the photon-induced generation of hot electrons in plasmonic particles reduces the activation energy for CO_2 hydrogenation.[25] Gunasooriya et al. used density functional theory (DFT) calculations and demonstrated that surface charges effectively reduce the binding energy (BE) of hydrocarbons on Pt.[26] Plasma etching, an established application of low-temperature plasmas, harnesses the momentum transfer from ions accelerated in the sheath to enhance surface reaction rates.[27] To summarize, nonthermal plasmas can provide multiple reaction pathways, both in the gas phase and at exposed surfaces. Unfortunately, the relative importance of these processes in the context of plasma-mediated catalysis remains poorly characterized and understood.

In this study, we aim to advance our understanding of the kinetics of plasma-modified surface reactions by performing in situ FTIR measurements in combination with temperature-programmed desorption (TPD) of CO from Pt nanoparticles under exposure to argon plasma. We choose to utilize a midpressure (3.7 Torr) radio frequency (RF)-driven plasma as these conditions are conducive to a spatially uniform, steady plasma that impinges onto the catalyst surface in a much better-defined way than that for the case of DBD reactors. We generate the plasma in a nonreactive gas, argon, to eliminate gas-phase chemistry and isolate the role of plasma-induced effects on a fundamental reaction parameter: the adsorption energy of CO on Pt. We selected this molecule−catalyst combination because the CO−Pt system has been extensively studied both experimentally and computationally, making it ideal for fundamental surface science.[28−31] Controlling the desorption kinetics of CO is crucial for enhancing catalytic reactions in various important processes, such as CO oxidation,[32] CO_2 hydrogenation,[33] water−gas shift reaction,[34] and Fischer−Tropsch process.[35]

We find that plasma exposure results in a significant reduction in effective CO BE to Pt nanoparticle surfaces, with a BE reduction that scales with the plasma density. Moreover, deconvolution of the Pt−CO peak indicates that the under-coordinated (UC, Pt surface sites with coordination numbers <8) adsorption sites experience a larger decrease in BE compared to well-coordinated (WC, Pt surface sites with coordination numbers of 9) sites, i.e., $\Delta BE_{UC} > \Delta BE_{WC}$ under plasma exposure. To better interpret this result, we performed DFT calculations, confirming that UC sites are more sensitive to changes in the surface charge density, consistent with the experimental findings.

Our work provides direct, experimental evidence of nonthermal activation of adsorbates on metal catalyst surfaces under nonthermal plasma excitation, underscoring the importance of surface activation as opposed to gas-phase activation of molecules for nonthermal plasma catalysis. Plasmas can induce significant changes in the adsorbate BE and the relative reactivity of different surface sites, which often dictate catalytic reactivity for metal nanoparticles, confirming that they can enable reaction pathways that are not achievable in heat-based processes. From a practical point of view, this could be leveraged to prevent catalyst poisoning, with CO poisoning being a well-known issue in many heterogeneous

https://doi.org/10.1021/jacsau.4c00309
JACS Au 2024, 4, 2979−2988

catalytic processes. This study shows that plasma-activated heterogeneous catalysis, while complex, can be investigated at its most fundamental levels by careful selection of the adsorbate-catalyst couple, providing a template for future investigations of this class of processes. This approach can be leveraged to extract fundamental parameters such as adsorption energies under plasma exposure, which could then be utilized to develop microkinetic models optimized for the investigation of plasma-driven heterogeneous catalytic processes.

RESULTS AND DISCUSSION

TPD Monitored by In Situ FTIR under Plasma Exposure

We performed in situ TPD experiments using diffuse reflectance infrared Fourier transform spectroscopy (DRIFTS) to measure adsorbate coverage. The commercial environmental chamber (HVC-DRP-5, Harrick Scientific) is modified by removing one of the three KBr windows and by replacing it with a Pyrex tubular reactor (see Figure 1a,b). Argon flows through the tube, and a radiofrequency-powered electrode is wrapped around the tube to sustain the discharge. The argon flow rate is 20 sccm, while the pressure is 3.7 Torr. The reaction chamber is then heated with a ramp rate of 10 °C/min during all TPD experiments. The effective CO BE is obtained through Redhead analysis (Figure S1).[36] It is assumed that the BE is equivalent to the desorption activation barrier (adsorption is barrierless). The effective BE is extracted at the coverage where the maximum rate of desorption occurs. It is important to appreciate that plasmas may influence the CO desorption kinetics through different parallel mechanisms (discussed in detail below). This may include modifications to the kinetics of the thermal process or the introduction of entirely new reaction channels. The existence of nonequilibrium (electronically excited) processes at the surface may cause nonthermal desorption pathways that cannot be captured by the Redhead analysis. The BE extracted from Redhead analysis is, therefore, an effective CO BE, which encompasses all potential reaction pathways.

Figure S2a shows a photograph of the reactor with and without the catalyst powder loaded in it. The powder is pressed into the heater to make a small pellet. Figure S2b confirms that the Pt particles are ∼1 nm in size with the alumina support in the ∼20 nm size range. The scanning electron microscopy images of the loaded powder (Figure S2c) show a dense powder bed with a smooth surface. As discussed by Zakem and Christopher,[37] this configuration ensures that the IR signal is sensitive to the top surface. At the same time, there is minimal penetration of plasma within such a dense powder bed. This experimental setup allows for the specific probing of the plasma-affected surface layer. After loading, a pretreatment protocol (see Table S1) is implemented to ensure that the catalyst surface is clean and that the metal is fully reduced. FTIR spectra over 20 min confirm the stable chemisorption of CO on the Pt nanoparticles (Figure S3). Figure 1c presents the obtained DRIFTS spectra during a TPD experiment at 1 min intervals, showing the expected decrease in peak area (proportional to coverage) as temperature increases.

Upon igniting the plasma, we observe a small but measurable blue-shift of the CO FTIR peak (Figure S4), providing the first evidence of weakening of the CO BE on Pt. Figure 1d shows the decrease in the effective CO BE on Pt nanoparticles as a function of the actual RF input power used for plasma generation. The actual power to sustain the plasma is obtained by measuring the discharge RF voltage, current, and the phase difference between them.[38] We find that roughly 10−20% of the power provided by the RF power supply is coupled to the discharge, consistent with our previous experiences with these small plasma reactors. The BE, calculated through the Redhead equation, is 1.55 eV/molecule (=150 kJ/mol) without plasma. Readsorption of CO could cause inaccurate measurements of BE,[39] but we regard that it does not significantly occur in our reaction chamber due to a sufficiently high pumping rate and negligible penetration depth of IR photons. Qi et al. measured a similar BE of 1.4 eV/molecule (=136 kJ/mol) between CO and 2 nm Pt nanoparticles using the identical system.[40] Golibrzuch et al. investigated the BE through the velocity-selected residence time method and reported the BE being 1.47 eV (see Figure 10 in the ref 41). Ertl et al. measured a CO BE of 1.2 eV on a Pt(111) single-crystal surface at 50% coverage.[42] It is important to note that Pt single-crystal surfaces exhibit lower CO BE than small Pt particles because of the higher relative concentration of WC adsorption sites.[43]

As shown in Figure 1d, the BE decreases with increasing RF power as the sample is exposed to the plasma and then plateaus for RF powers above 2 W. At a plasma power of 1.6 W, the BE is decreased by ∼0.3 eV compared with the case without plasma. This shows that even a low-power plasma (1.6 W) in a nonreactive atmosphere can significantly enhance the kinetics of CO desorption, with the temperature at the maximum rate of desorption being ∼100 °C lower than that for the case without the plasma. We point out that strong chemisorption of CO, especially at low temperatures, has been shown to prevent CO_2 hydrogenation.[44] The plasma exposure, therefore, could offer a pathway to control surface reaction kinetics in a manner that cannot be achieved by thermal activation alone. We stress that the CO desorption kinetics in this system can only be influenced by plasma−surface interactions, distinct from the plasma-induced gas phase excitation often assumed in nonthermal plasma-promoted catalysis studies.

Plasma Density Measurements

We performed capacitive probe measurements to estimate the plasma density and investigate its effect on the Pt−CO BE.[45] Plasma density is an intrinsic property of the system, therefore providing a more reliable metric than input power to compare different reactors. Figure S5 shows the measured ion density as a function of the RF input power. We find that the ion density increases with increasing power in the low-power regime and remains nearly constant at power levels above 2 W. While the plasma density is expected to increase with input RF power, it is also known to do so with a nontrivial relation that is affected by the reactor geometry. Most importantly, the plot of the BE as a function of the measured plasma density (Figure 1e) shows a nearly linear relationship. This strongly supports the conclusion that the BE can be tuned by controlling the plasma impinging onto the catalyst-adsorbate couple.

As mentioned earlier, plasmas may influence surface reaction kinetics through different parallel mechanisms, including thermalization of plasma-produced species at the exposed surfaces. This results in localized heating at the surface. Previous in-operando Raman thermometry measurements showed that the surface temperature of graphene increases by as much as 160 °C at an RF power of 5 W in an argon

https://doi.org/10.1021/jacsau.4c00309
JACS Au 2024, 4, 2979−2988

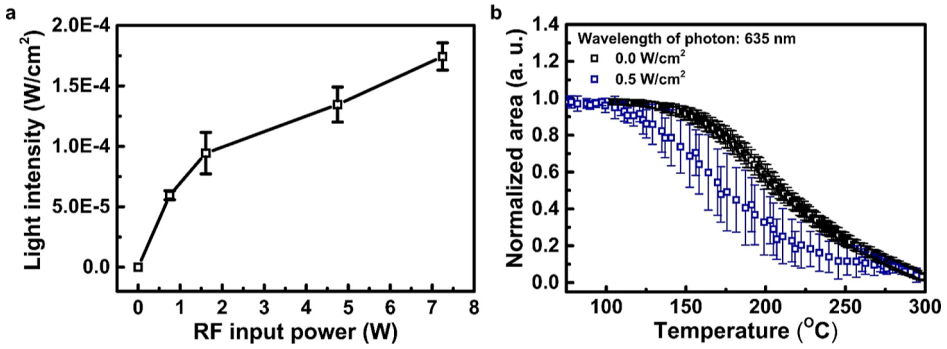

Figure 2. Comparison of photon irradiation from the plasma and the laser. (a) Light intensity as a function of the measured RF input power. Light intensity measurements have been performed three times to determine error bars. (b) TPD data under dark conditions and 635 nm light exposure (BE for dark mode: 1.4 eV and BE with light exposure: 1.3 eV). Light intensity from the Ar plasma is much weaker than that of the 635 nm laser. These results suggest that plasma-induced photon irradiation cannot account for the desorption of CO in this system.

plasma.[46] We recently repeated this measurement for the case of a self-assembled molecular monolayer and again found significant localized heating of the surface.[47] We stress that those measurements were performed with the same setup utilized for this study.[46,47] While the localized heating effect is certainly present, it is also not sufficient to explain the measured kinetics of the desorption of CO from Pt. A purely thermal effect would induce a shift in the peak desorption temperature. Figure 1f shows that the desorption peak moves to a lower temperature but the TPD spectrum also becomes significantly narrower under plasma exposure, suggesting that a thermal effect alone cannot explain the experimental observation.

CO BE is coverage-dependent because CO−CO repulsive forces tune the interaction between CO and the Pt surface, resulting in the broadening of the desorption peak.[48,49] Shan et al. reported the reduction in BE as a function of the CO coverage through DFT calculations, indicating that higher coverage led to a lower BE.[50] This has also been confirmed experimentally.[42] The narrowing of the peak in Figure 1f suggests that the desorption of CO is less coverage-dependent when irradiated by the argon plasma, consistent with it being enhanced by the flux of plasma-produced species onto the catalyst surface. Figure S6 suggests that desorption of CO rapidly occurs at lower temperatures with argon plasma exposure.

There is an abundance of reports suggesting that light can drive surface chemistry on metal surfaces.[25,35] The CO−Pt bond can be selectively activated by resonant photoexcitation of electronic transitions between bonding and antibonding states.[51] Therefore, we proceed to assess whether plasma-produced photons can indeed reduce the BE in the Pt−CO system.[52]

Light-Induced Effect

Figure 2a presents the measured light intensity as a function of the RF input power. The light intensity increases with the RF input power, reaching the highest light intensity at 1.7×10^{-4} W/cm^2 at the highest RF power. As expected, the dependence in Figure 2 closely resembles the trend of the plasma density with RF power. Still, the photon irradiance from the argon plasma is much smaller than typically used fluxes in studies of photochemistry/catalysis on supported metal catalysts (>100 mW/cm^2). Consistent with this hypothesis, control measurement of BE under laser irradiation suggests that a power of 0.5 W/cm^2 at 635 nm is needed to induce a ∼0.1 eV reduction in effective BE, as shown in Figure 2b. This photon flux is orders of magnitude higher than that supplied by the nonthermal argon plasma, at least in our discharge configuration. We conclude that the contribution from plasma-produced photons to the reduction in the BE is negligible for this system.

Overall, these results suggest that plasma exposure leads to a significant decrease in the effective BE of CO to Pt. Localized heating effects at the catalyst surface likely contribute to the decrease, although the kinetics of desorption strongly point to the importance of nonthermal effects in this system. We can rule out a major contribution from photochemical effects induced by plasma-generated radiation. Other mechanisms often hypothesized to affect surface chemistry in plasma catalysis are fluxes of charged species, charging, and strong electric fields at the catalyst surface. To the best of our knowledge, experiments that can fully resolve the relative importance of these mechanisms have yet to be designed and executed. The strong coupling among them makes it particularly challenging to probe these systems experimentally. Nevertheless, we leverage the properties of the Pt−CO system to gain insights into how plasma affects different bonding sites on the surface of a nanoparticle Pt catalyst. With the aid of the DFT calculation, we can conclusively attribute this phenomenon to the combination of surface charging and electric fields.

Selective Activation of Under-Coordinated Sites

Exposure to an argon nonthermal plasma affects not only the BE of CO on Pt but also the depletion in CO coverage at distinct sites on the Pt nanoparticle surface. We deconvoluted the FTIR peak to resolve the contribution from WC (Pt surface atoms with a coordination number of 9 to neighboring Pt, e.g., terrace sites) and UC (Pt surface atoms with a coordination number of <8 to neighboring Pt, e.g., step and edge sites) sites (Figure S7). We do so by using broadly accepted band assignments that attribute the 2065−2080 cm^{-1} band to CO adsorbed on WC sites and the 2050−2060 and 2030−2045 cm^{-1} bands to under-coordinated sites labeled as UC1 and UC2, respectively.[28,53] Although direct measurements of the distribution of Pt surface site coordination numbers are not possible, previous studies have demonstrated that surface Pt coordination numbers can be inferred from CO probe molecule DRIFT measurement.[28]

We estimated the BE of the CO to each site from the TPD curve using the Redhead equation. Figure S8 shows the fitting for both WC and UC sites based on the presence or absence of plasma exposure with increasing temperature. We find that the

https://doi.org/10.1021/jacsau.4c00309
JACS Au 2024, 4, 2979−2988

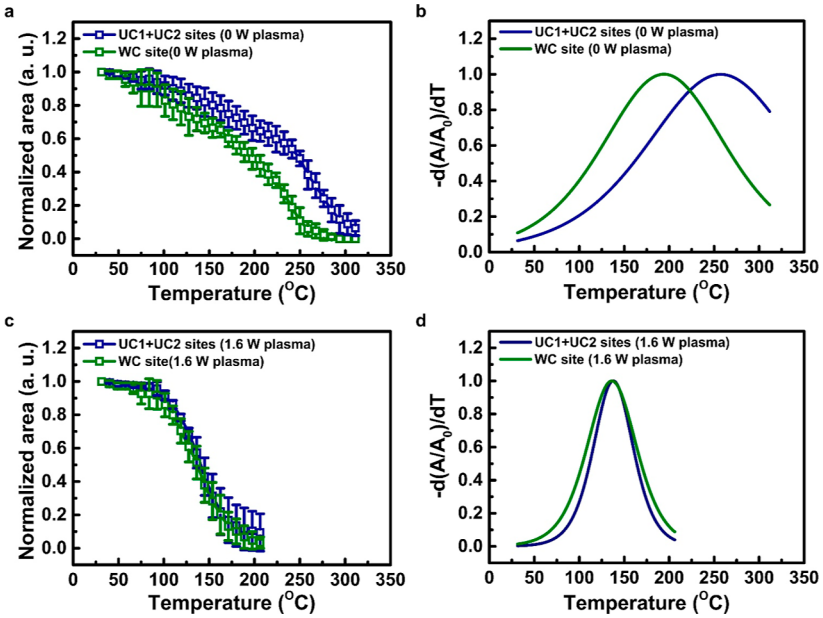

Figure 3. Selective desorption of CO with the Ar plasma. (a,b) Normalized area (A/A_0) obtained by integrating the FTIR spectrum and its derivative with respect to temperature for the UC and WC sites without plasma. (c,d) Same quantities but with the 1.6 W Ar plasma. The change in BE of the UC site is larger than that of the WC site (ΔBE_{UC}: 0.37 eV and ΔBE_{WC}: 0.19 eV), indicating that the Ar plasma promotes the activation of CO on the UC site more than that on the WC site.

BE for CO adsorbed onto UC2 sites is very close to that of UC1 sites (Figure S9). We therefore proceed to sum the integrated areas of both UC1 and UC2 sites and simply treat them as under-coordinated (UC) sites. We have performed this fitting three times for each separate data set to determine the standard deviation. It is important to note that fast diffusion of CO between UC and WC occurs, and thus, the site-specific BEs represent the binding site-specific preference of CO. In the absence of the argon plasma, the UC site has higher BE than that of the WC site, as shown in Figure 3a (BE_{UC} = 1.58 ± 0.03 eV/molecule = 153 ± 3 kJ/mol and BE_{WC} = 1.40 ± 0.02 eV/molecule = 136 ± 2 kJ/mol). The temperature at the maximum rate of desorption (T_{max}) shows an ∼60 °C difference between the WC and UC sites, as exhibited in Figure 3b. This is consistent with literature reports and expectations based on the d-band model.[54,55] For instance, Kalff et al. reported the activation energies for desorption of the step site (UC site) and the terrace site (WC site) as 1.7 eV/molecule (=165 kJ/mol) and 1.4 eV/molecule (=136 kJ/mol), respectively.[56]

Figure 3c shows the CO BE at UC and WC sites with exposure to the argon plasma, with corresponding values of 1.21 ± 0.02 eV/molecule (=117 ± 2 kJ/mol) for both UC and WC sites. The difference in T_{max} between the UC and WC sites reduces from ∼60 ± 8 °C to almost zero under plasma exposure, as presented in Figure 3d. This confirms that the change in BE is larger at the UC site compared to the WC site, i.e., $\Delta BE_{UC} > \Delta BE_{WC}$. Plasma exposure can therefore markedly change the relative site preference of CO on Pt away from the strong preference for UC sites without plasma exposure.

The electrical double layer, or sheath, in front of plasma-exposed surfaces inevitably leads to surface charging and electric field formation. Previous theoretical work has suggested that charging can indeed tune the BE of surface adsorbates, which can be surface site-specific.[57−59] Onn et al. recently measured change in BE of CO adsorbed on the UC sites of Pt nanoclusters (see Figure 5b in the ref 60) via a catalytic condenser device capable of inducing electron or hole accumulation on the Pt active sites.[60] Motivated by these considerations, we performed atomistic simulations to explore the role of surface charging on both the UC and WC sites and to compare the theoretical results with our measurements.

DFT Calculations

We calculated the effect of surface charging on the BE of CO to Pt using the CP2K[61,62] software package. The computational details are given in the Methods section of this manuscript. We followed the approach proposed by Bal and Neyts[63] to model the surface charging induced by a plasma. In this approach, the additional negative charge placed onto the slab's surface is compensated by a proton positioned within the vacuum layer, thereby preserving the overall charge neutrality. This technique has been accepted by the plasma community as a viable representation of the environment created by a nonthermal plasma interacting with a catalyst surface. Bal et al. used it to model the effect of charging for the case of CO_2 adsorption onto Ti, Ni, and Cu catalysts.[57] Similarly, Jafarzadeh et al. used the same strategy to model the activation of CO_2 on copper surfaces, finding that charging in this case leads to an increase in adsorption energy.[58,64] In our case, the (111) and (211) facets of Pt are used to model the WC and UC sites, respectively. For these calculations, the proton sits at a distance of 25 Å from the surface. The addition of a single negative charge to the surface corresponds to an average charge density of −0.05 C/m^2 for the (111) surface and −0.07 C/m^2 for the (211) surface. Figure 4 illustrates different CO adsorption configurations, along with the associated BE in both neutral and charged environments. Under neutral conditions (Figure 4a), the BE of CO on the WC Pt(111) is 2.24 eV/molecule (=217 kJ/mol). However, a stronger BE is observed on the UC Pt(211) surface under a similar condition (Figure 4d), with a BE of 2.69 eV/molecule (=260 kJ/mol). This is in good agreement with published results.[54−56] The prediction

https://doi.org/10.1021/jacsau.4c00309
JACS Au 2024, 4, 2979−2988

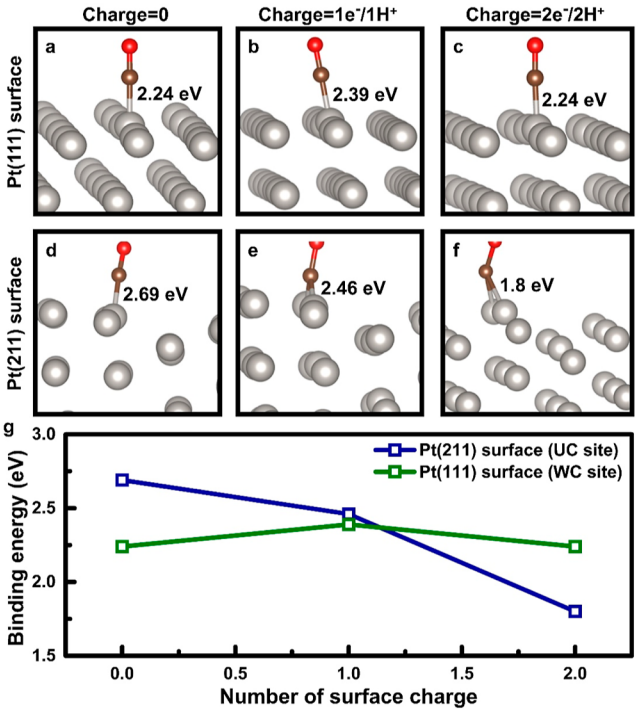

Figure 4. Various adsorption configurations of the CO on Pt(111) and Pt(211) surfaces. (a,d) Stronger adsorption of CO on the neutral Pt(211) surface rather than the Pt(111) surface. (b,e) One surface charge. (c,f) Two surface charges on both Pt(111) and Pt(211). (g) Change in BE of Pt(111) and Pt(211) surfaces as a function of the number of surface charges. Interestingly, while the BE of Pt(111) surface remains nearly constant regardless of the negative charges induced on the surface, the BE of Pt(211) surface is significantly reduced in the presence of surface charges.

from DFT calculations of a stronger BE than that observed in the experiments is most likely due to the choice of exchange–correlation functional and the effect of coverage. The Redhead analysis extracts the BE from the temperature at which the desorption rate is at its maximum, corresponding to ∼50% surface coverage. Still, the DFT calculations successfully predicted the relative BE of CO on WC and UC sites, consistent with our measurements.

On the Pt(111) surface, the charged environment predicts a slightly stronger BE for CO (Figure 4b) compared to neutrality. In contrast, a reverse trend emerges for the Pt(211) surface with the BE of CO being weaker on the charged surface (Figure 4e) relative to the uncharged state (Figure 4d). Figure 4c depicts the adsorption configuration of CO on Pt(111) with $2e^-$ charges on the surface, yielding a BE of 2.24 eV/molecule (=217 kJ/mol). Notably, the BE for CO on the Pt(211) surface with $2e^-$ charges (Figure 4f) experiences a significant reduction compared to neutral and singly charged surfaces, with BE decreasing to 1.8 eV/molecule (=175 kJ/mol). These results are summarized in Figure 4g, showing that the Pt(211) surface, which is a proxy for UC surface sites, is much more sensitive to surface charging than the Pt(111) surface, i.e., WC sites. This is in good agreement with the experimental results shown in Figure 4.

We assessed the role played by the electric field by calculating the BE of CO on Pt(111) and Pt(211) surfaces while varying the distance of the counterion from the surface. Supporting Information includes adsorption configurations of CO on Pt(111) and Pt(211) surfaces with $1e^-/1H^+$ charges at a distance of 40 Å (i.e., weaker electric field compared to the 25 Å case) above the surface, yielding adsorption energies of 2.19 eV/molecule (=213 kJ/mol, Figure S10a) and 2.52 eV/molecule (=244 kJ/mol, Figure S10b), respectively. These values are close to those for the neutral system, underscoring how both charging and electric fields contribute to the reduction in BE, especially for the UC sites.

It is important to note that the combination of surface charge and electric field explains the relative change in the BE for the WC and UC sites. Still, the DFT calculations show that charging does not strongly affect the BE for the WC sites, while our measurements show a decrease in the BE for these sites as well under plasma exposure. As mentioned earlier, this could be explained by the localized release of energy at the plasma-exposure surfaces. Other mechanisms, such as the flux of charged species to the surface, could play a role here as well. Reports suggest that the electron flux generated by a scanning tunneling probe can induce chemical changes in the case of CO- or CO_2-covered metal surfaces.[65,66] Our findings are consistent with those recently reported by Xu et al., who observed an enhancement of CO_2 hydrogenation through less CO poisoning by nonthermal plasma surface activation.[9] Finally, the fact that we effectively measure the same BE for WC and UC sites under plasma exposure is consistent with the rapid migration of CO from terraces to steps, where the

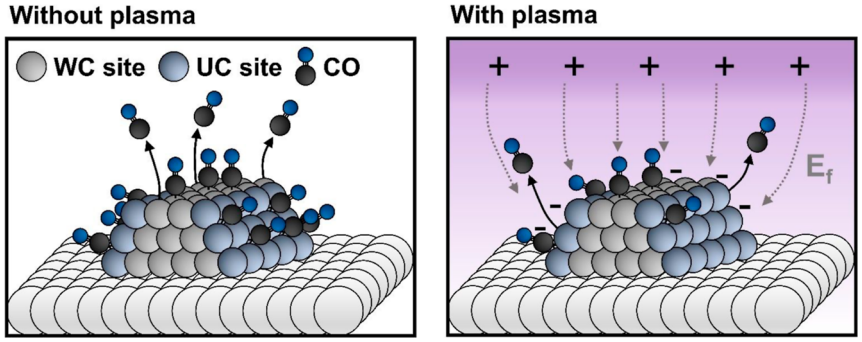

Figure 5. Selectively desorbed CO on the UC site of Pt nanoparticles under Ar plasma exposure. The schematic shows that the BE for the UC sites is higher than that of the WC sites in the absence of argon plasma exposure (left panel). With the argon plasma exposure (right panel), surface charging and electric field promote selective activation of CO of the UC site. The low activation energy for the diffusion of CO on Pt (∼0.2 eV) suggests that CO adsorbed on the WC sites migrates to the vacant UC sites, resulting in almost the same BE for both sites with argon plasma exposure.

https://doi.org/10.1021/jacsau.4c00309
JACS Au 2024, 4, 2979–2988

combination of charging and the electric field reduces the BE strongly. We point out that the activation energy of surface diffusion for CO on Pt is relatively low (~0.2 eV).

CONCLUSIONS

We utilized TPD to perform an in-depth investigation of how a nonthermal plasma affects the desorption of CO from Pt nanoparticles. Overall, the nonthermal plasma induces a significant reduction in BE, which scales linearly with the plasma density. This opens the possibility of using a nonthermal plasma to mitigate the CO-induced poisoning of the catalyst surface. The thermalization of plasma-produced species at the exposed catalyst surface, which leads to surface-localized heating, most likely contributes to the decrease in the temperature at the maximum rate of desorption, although this thermal effect alone cannot explain the measured kinetics of desorption. The considerable narrowing of the temperature interval in which desorption takes place suggests that the process is much less surface coverage dependent on plasma exposure. While the flux of plasma-produced species to the catalyst surface may contribute to the reduction in BE, we find that plasma-generated photons do not play a significant role in decreasing BE. Most importantly, we have found that plasma exposure strongly affects the relative activity of different surface sites on the Pt nanoclusters, with the decrease in BE being considerably more significant for the under-coordinated sites compared to the well-coordinate ones, as graphically summarized in Figure 5. DFT calculations confirm that the undercoordinate sites are much more sensitive to surface charging and electric fields compared to well-coordinate sites.

Overall, this work suggests that nonthermal plasmas strongly affect the kinetics of fundamental surface processes. These effects play a major role in tuning the activity and selectivity of catalysts under plasma exposure. These effects should be included in the microkinetics models that already incorporate plasma-induced gas-phase excitation and that are broadly utilized by the community. Accounting for these effects would likely improve the interpretation of reactor-level behavior. While this work provides mechanistic insights into the microscopic phenomena occurring at the plasma−catalyst interface, continued efforts should be devoted to the design of experiments and models that can address how different plasma-produced species (e.g., electrons and ions) affect the rate of surface reactions.

METHODS

Catalyst Preparation

The 1% Pt/Al_2O_3 catalyst was synthesized by impregnating gamma alumina (γ-Al_2O_3 99.99% purity, 20 nm particle size, SkySpring Nanomaterials Inc.) with tetraammineplatinum(II) nitrate ($Pt(NH_3)_4(NO_3)_2$, 99.995% purity, trace metal basis, Sigma-Aldrich). For the synthesis of 1 g of the catalyst, 0.02 g of $Pt(NH_3)_4(NO_3)_2$ was dissolved in 3.0 mL of high-performance liquid chromatography grade H_2O, resulting in a uniform solution. The solution of $Pt(NH_3)_4(NO_3)_2$ was then combined with 0.99 g of γ-Al_2O_3, creating a white slurry. Afterward, the catalyst was dried at 100 °C overnight to remove any excess water, followed by calcination at 600 °C in the presence of airflow for 6 h.

TPD Experiments

The schematic and picture of our experimental system are shown in Figure 1a,b. TPD experiments were carried out using a high-temperature reaction chamber through DRIFTS. The reaction chamber was equipped inside a Praying Mantis diffuse reflectance adapter (DRP-XXX, Harrick Scientific). The adapter was then mounted on a FTIR spectrometer (iS50, Thermo Fisher Scientific). All spectra were obtained using a reduced catalyst bed as a background, utilizing a liquid-nitrogen-cooled HgCdTe detector and averaging 16 scans at a resolution of 4 cm^{-1}. All temperatures used in this study were calibrated using a thermocouple in order to accurately represent the temperature of the catalyst surface (Figure S11). We did a strict pretreatment to fully reduce the catalyst before all TPD experiments (Table S1). Once the pretreatment was completed, a background FTIR spectrum was obtained at room temperature without any CO exposure; then chemisorption of CO occurred at room temperature when flowing 10 sccm of CO and 20 sccm of Ar for 10 min. Prior to the initiating TPD experiments, the reaction chamber was flushed through 20 sccm of Ar gas for 3 min to remove any remaining gas-phase CO in the chamber. During all TPD experiments, the pressure was maintained at 3.7 Torr. The flow rate of Ar was kept at 20 sccm. We set the ramp rate at 10 °C/min by using a temperature controller (ATK-024-3, Harrick Scientific). The obtained spectra were baseline corrected to remove broad shifts in the spectra that did not affect the shape of the CO peak.

One of the KBr windows was replaced by a plasma reactor with a diameter of 5.4 mm for Ar plasma irradiation (Figure 1b). The RF-biased electrode was covered outside of the reactor tube and powered by a power supply (RFPP RF-5S, Advanced Energy). The electrical impedance was matched through a matching network (MFJ-989D, MFJ). The Ar plasma was ignited with the 20 sccm of Ar flow. The flow rate of gases was controlled by mass flow controllers (MKS 1179C, MKS Instruments).

Light Intensity Measurements

Light intensity was measured by using a Si-biased detector (DET10A, Thorlabs) by reading the voltage through an oscilloscope (TES2024C Tektronix). We mounted the detector outside one of the KBr windows and then obtained current from the measured voltage using Ohm's law (resistance = 1 MΩ). We used a responsivity of 0.328 A/W when converting the current to power, considering that the Ar plasma emits photons of various wavelengths (Figure S12). The signal intensity is corrected to account for the ~90% transmissivity of the KBr window.

Plasma Density Measurements

The capacitive probe measurements were conducted to measure the ion density of the Ar plasma. The probe was inserted into the reaction chamber through one of the KBr windows. A copper wire with a diameter of 2.5 mm and a length of 0.5 mm was employed as a probe tip and connected to a 200 pF capacitor and an RF power supply (RFPP RF-5S, Advanced Energy) capable of pulsed operation. The capacitor voltage was measured through an oscilloscope (TES2024C Tektronix). The RF power supply charged the capacitor negatively via the pulse. The capacitor then discharged due to the ion flux from the Ar plasma toward the probe (Figure S13).

We assumed that Ar ions enter the sheath edge with Bohm velocity. To calculate the Bohm velocity, it is necessary to know the electron temperature. The electron temperature was estimated by balancing the rates of ionization (as obtained by Bolsig+) and wall losses.[67] Our previous report summarized this method well.[11] We obtained a value of electron temperature of 5.5 eV, independent of the RF power.

DFT Calculations

Utilizing the CP2K[61,62] software package, we carried out DFT calculations. Energies and forces were determined using the Gaussian and plane wave method,[68] incorporating GTH pseudopotentials[69,70] to account for core−valence interactions. A double-ζ valence potential basis set was utilized to expand the Kohn−Sham valence orbitals. An auxiliary plane wave basis set of 500 Ry was defined to model the electron density. The DFT calculation employed the PBE[71] functional for exchange and correlation, supplemented by Grimme's D3 dispersion correction in its Becke−Jhonson damping form.[72] Our calculations were carried out with Pt(111) and Pt(211) surfaces for CO adsorption (Figure S14). A 3 × 2 × 1 slab was utilized to model the Pt(111) and Pt(211) surfaces, where the bottom two layers of

https://doi.org/10.1021/jacsau.4c00309
JACS Au 2024, 4, 2979−2988

each substrate were fixed to correspond with the bulk lattice configuration.

A simplistic approach to simulate a charged catalyst surface involves the addition of an electron directly to the surface, inducing a negative charge. However, this method is unsuitable due to the divergence of the electrostatic energy in periodically replicated charged systems, which defies physical reality. Conventional electronic structure techniques circumvent this issue by placing the charged system in a neutral background charge. Nevertheless, this strategy becomes inadequate with systems characterized by a nonuniform distribution of countercharge.[73] We introduce a positive countercharge onto the negatively charged surface with the CP2K code.[61,62] The proton represents the most straightforward choice for this countercharge. The approach yields a credible depiction of a charged catalyst surface exposed to plasma due to two critical factors: (1) it realistically depicts a negatively charged surface in contact with a gas phase carrying positive countercharges, and (2) it spontaneously generates an electric field perpendicular to the surface. We implemented this approach using the methodology by Bal and Neyts,[63] i.e., by introducing an additional electron charge to the slab's surface while compensating it with a proton positioned within the vacuum layer, thereby preserving the overall charge neutrality. Notably, the H^+ counterion was assigned a null basis set, ensuring its isolation from interactions with other system atoms. This strategic decision directed the surplus electron to associate primarily with the surface rather than with the H^+ entity itself. In charged systems, the proton counterion was positioned approximately 25 Å above the surface, and the total cell height of 100 Å was used. Similarly, a total cell height of 100 Å was also employed for uncharged systems. Within our simulations, we employed the Martyna–Tuckerman (MT) solver,[74] enabling the imposition of two periodic directions (aligned with the surface in the *xy*-plane) and one nonperiodic direction (corresponding to the surface normal in the *z*-direction). The MT solver serves as a reciprocal space-driven technique for evaluating electrostatic energies, accommodating the treatment of both isolated and periodically replicated systems within a unified framework.

■ ASSOCIATED CONTENT

Supporting Information

The Supporting Information is available free of charge at https://pubs.acs.org/doi/10.1021/jacsau.4c00309.

Details of Redhead analysis, catalyst characterization, TPD experiments, light intensity and plasma density measurements, deconvolution for CO peak, and DFT calculations (PDF)

■ AUTHOR INFORMATION

Corresponding Authors

Phillip Christopher − *Department of Chemical Engineering, University of California, Santa Barbara, Santa Barbara, California 93117, United States;* orcid.org/0000-0002-4898-5510; Email: pchristopher@ucsb.edu

Bryan M. Wong − *Materials Science & Engineering Program, University of California, Riverside, Riverside, California 92521, United States;* orcid.org/0000-0002-3477-8043; Email: bryan.wong@ucr.edu

Lorenzo Mangolini − *Department of Mechanical Engineering, University of California, Riverside, Riverside, California 92521, United States; Materials Science & Engineering Program, University of California, Riverside, Riverside, California 92521, United States;* orcid.org/0000-0002-0057-2450; Email: lmangolini@engr.ucr.edu

Authors

Minseok Kim − *Department of Mechanical Engineering, University of California, Riverside, Riverside, California 92521, United States*

Sohag Biswas − *Materials Science & Engineering Program, University of California, Riverside, Riverside, California 92521, United States*

Isabel Barraza Alvarez − *Department of Chemistry and Biochemistry, University of California, Santa Barbara, Santa Barbara, California 93117, United States*

Complete contact information is available at: https://pubs.acs.org/10.1021/jacsau.4c00309

Author Contributions

M.K. performed the TPD measurements under thermal and plasma activation and plasma characterization, analyzed the data, drafted, and finalized the manuscript. S.B. and B.M.W. performed the DFT calculation and drafted the corresponding section in the manuscript. I.B.A. and P.C. performed the TPD measurements under laser irradiation and assisted with the data analysis and interpretation. L.M. advised M.K. and assisted with the data analysis and with finalizing the manuscript.

Notes

The authors declare no competing financial interest.

■ ACKNOWLEDGMENTS

This work has been primarily supported by the U.S. Department of Energy, National Energy Technology Laboratory (DOE-NETL) under award number DEFE0032091. M.K. acknowledges the support from the Hyundai Motor Chung Mong-Koo Foundation, Republic of Korea. P.C. and I.B.A. acknowledge support from the Army Research Office PECASE Grant W911NF-19-1−0116. I.B.A. also acknowledges support from the National Science Foundation Graduate Research Fellowship Program (NSF GRFP) under grant no. 2139319.

■ REFERENCES

(1) Chen, J. G.; Crooks, R. M.; Seefeldt, L. C.; Bren, K. L.; Morris Bullock, R.; Darensbourg, M. Y.; Holland, P. L.; Hoffman, B.; Janik, M. J.; Jones, A. K.; Kanatzidis, M. G.; King, P.; Lancaster, K. M.; Lymar, S. V.; Pfromm, P.; Schneider, W. F.; Schrock, R. R. Beyond Fossil Fuel-Driven Nitrogen Transformations. *Science* **2018**, *360*, No. eaar6611.

(2) Barton, J. L. Electrification of the Chemical Industry. *Science* **2020**, *368* (6496), 1181−1182.

(3) Luderer, G.; Madeddu, S.; Merfort, L.; Ueckerdt, F.; Pehl, M.; Pietzcker, R.; Rottoli, M.; Schreyer, F.; Bauer, N.; Baumstark, L.; Bertram, C.; Dirnaichner, A.; Humpenöder, F.; Levesque, A.; Popp, A.; Rodrigues, R.; Strefler, J.; Kriegler, E. Impact of Declining Renewable Energy Costs on Electrification in Low-Emission Scenarios. *Nat. Energy* **2022**, *7* (1), 32−42.

(4) Winter, L. R.; Chen, J. G. N_2 Fixation by Plasma-Activated Processes. *Joule* **2021**, *5* (2), 300−315.

(5) Lee, B.; Winter, L. R.; Lee, H.; Lim, D.; Lim, H.; Elimelech, M. Pathways to a Green Ammonia Future. *ACS Energy Lett.* **2022**, *7* (9), 3032−3038.

(6) Nozaki, T.; Okazaki, K. Non-Thermal Plasma Catalysis of Methane: Principles, Energy Efficiency, and Applications. *Catal. Today* **2013**, *211*, 29−38.

(7) Wang, L.; Yi, Y.; Wu, C.; Guo, H.; Tu, X. One-Step Reforming of CO_2 and CH_4 into High-Value Liquid Chemicals and Fuels at Room

Temperature by Plasma-Driven Catalysis. *Angew. Chem., Int. Ed.* **2017**, *56* (44), 13679−13683.
(8) Bogaerts, A.; Neyts, E. C. Plasma Technology: An Emerging Technology for Energy Storage. *ACS Energy Lett.* **2018**, *3* (4), 1013−1027.
(9) Xu, S.; Chansai, S.; Xu, S.; Stere, C. E.; Jiao, Y.; Yang, S.; Hardacre, C.; Fan, X. CO Poisoning of Ru Catalysts in CO_2 Hydrogenation under Thermal and Plasma Conditions: A Combined Kinetic and Diffuse Reflectance Infrared Fourier Transform Spectroscopy-Mass Spectrometry Study. *ACS Catal.* **2020**, *10* (21), 12828−12840.
(10) Yamijala, S. S. R. K. C.; Nava, G.; Ali, Z. A.; Beretta, D.; Wong, B. M.; Mangolini, L. Harnessing Plasma Environments for Ammonia Catalysis: Mechanistic Insights from Experiments and Large-Scale Ab Initio Molecular Dynamics. *J. Phys. Chem. Lett.* **2020**, *11* (24), 10469−10475.
(11) Kim, M.; Biswas, S.; Nava, G.; Wong, B. M.; Mangolini, L. Reduced Energy Cost of Ammonia Synthesis Via RF Plasma Pulsing. *ACS Sustain. Chem. Eng.* **2022**, *10* (46), 15135−15147.
(12) Ma, H.; Sharma, R. K.; Welzel, S.; van de Sanden, M. C. M.; Tsampas, M. N.; Schneider, W. F. Observation and Rationalization of Nitrogen Oxidation Enabled Only by Coupled Plasma and Catalyst. *Nat. Commun.* **2022**, *13*, 402.
(13) Sheng, Z.; Watanabe, Y.; Kim, H. H.; Yao, S.; Nozaki, T. Plasma-Enabled Mode-Selective Activation of CH_4 for Dry Reforming: First Touch on the Kinetic Analysis. *Chem. Eng. J.* **2020**, *399* (1), 125751.
(14) Snoeckx, R.; Bogaerts, A. Plasma Technology - a Novel Solution for CO_2 Conversion? *Chem. Soc. Rev.* **2017**, *46*, 5805−5863.
(15) Rouwenhorst, K. H. R.; Jardali, F.; Bogaerts, A.; Lefferts, L. From the Birkeland-Eyde Process towards Energy-Efficient Plasma-Based NO: Xsynthesis: A Techno-Economic Analysis. *Energy Environ. Sci.* **2021**, *14* (5), 2520−2534.
(16) Chen, X.; Kim, H. H.; Nozaki, T. Plasma Catalytic Technology for CH_4 and CO_2 Conversion: A Review Highlighting Fluidized-Bed Plasma Reactor. *Plasma Processes Polym.* **2023**, *21* (1), 2200207.
(17) Shah, J.; Wang, W.; Bogaerts, A.; Carreon, M. L. Ammonia Synthesis by Radio Frequency Plasma Catalysis: Revealing the Underlying Mechanisms. *ACS Appl. Energy Mater.* **2018**, *1* (9), 4824−4839.
(18) Engelmann, Y.; Van'T Veer, K.; Gorbanev, Y.; Neyts, E. C.; Schneider, W. F.; Bogaerts, A. Plasma Catalysis for Ammonia Synthesis: A Microkinetic Modeling Study on the Contributions of Eley-Rideal Reactions. *ACS Sustain. Chem. Eng.* **2021**, *9* (39), 13151−13163.
(19) Mehta, P.; Barboun, P.; Herrera, F. A.; Kim, J.; Rumbach, P.; Go, D. B.; Hicks, J. C.; Schneider, W. F. Overcoming Ammonia Synthesis Scaling Relations with Plasma-Enabled Catalysis. *Nat. Catal.* **2018**, *1* (4), 269−275.
(20) Kim, J.; Abbott, M. S.; Go, D. B.; Hicks, J. C. Enhancing C-H Bond Activation of Methane via Temperature-Controlled, Catalyst-Plasma Interactions. *ACS Energy Lett.* **2016**, *1* (1), 94−99.
(21) Kim, D. Y.; Ham, H.; Chen, X.; Liu, S.; Xu, H.; Lu, B.; Furukawa, S.; Kim, H. H.; Takakusagi, S.; Sasaki, K.; Nozaki, T. Cooperative Catalysis of Vibrationally Excited CO_2 and Alloy Catalyst Breaks the Thermodynamic Equilibrium Limitation. *J. Am. Chem. Soc.* **2022**, *144* (31), 14140−14149.
(22) Li, Y.; Hinshelwood, M.; Oehrlein, G. S. Investigation of Ni catalyst activation during plasma-assisted methane oxidation. *J. Phys. D: Appl. Phys.* **2022**, *55*, 155202.
(23) Kim, D. Y.; Saito, A.; Sasaki, K.; Nozaki, T. In Situ Infrared Absorption Probing of Plasma Catalysis: Vibrationally-Excited Species Induced Mars-van Krevelen Type Mechanism. *Plasma Sources Sci. Technol.* **2022**, *31*, 124005.
(24) Xu, S.; Chansai, S.; Shao, Y.; Xu, S.; Wang, Y. c.; Haigh, S.; Mu, Y.; Jiao, Y.; Stere, C. E.; Chen, H.; Fan, X.; Hardacre, C. Mechanistic Study of Non-Thermal Plasma Assisted CO2 Hydrogenation over Ru Supported on MgAl Layered Double Hydroxide. *Appl. Catal., B* **2020**, *268*, 118752.
(25) Zhang, X.; Li, X.; Zhang, D.; Su, N. Q.; Yang, W.; Everitt, H. O.; Liu, J. Product Selectivity in Plasmonic Photocatalysis for Carbon Dioxide Hydrogenation. *Nat. Commun.* **2017**, *8*, 14542.
(26) Gunasooriya, G. T. K. K.; Seebauer, E. G.; Saeys, M. Ethylene Hydrogenation over Pt/TiO_2: A Charge-Sensitive Reaction. *ACS Catal.* **2017**, *7* (3), 1966−1970.
(27) Donnelly, V. M.; Kornblit, A. Plasma Etching: Yesterday, Today, and Tomorrow. *J. Vac. Sci. Technol. A* **2013**, *31*, 050825.
(28) Kale, M. J.; Christopher, P. Utilizing Quantitative in Situ FTIR Spectroscopy to Identify Well-Coordinated Pt Atoms as the Active Site for CO Oxidation on Al_2O_3-Supported Pt Catalysts. *ACS Catal.* **2016**, *6* (8), 5599−5609.
(29) Thang, H. V.; Pacchioni, G.; DeRita, L.; Christopher, P. Nature of Stable Single Atom Pt Catalysts Dispersed on Anatase TiO_2. *J. Catal.* **2018**, *367*, 104−114.
(30) Gunasooriya, G. T. K. K.; Saeys, M. CO Adsorption on Pt(111): From Isolated Molecules to Ordered High-Coverage Structures. *ACS Catal.* **2018**, *8* (11), 10225−10233.
(31) Sumaria, V.; Nguyen, L.; Tao, F. F.; Sautet, P. Optimal Packing of CO at a High Coverage on Pt(100) and Pt(111) Surfaces. *ACS Catal.* **2020**, *10* (16), 9533−9544.
(32) Allian, A. D.; Takanabe, K.; Fujdala, K. L.; Hao, X.; Truex, T. J.; Cai, J.; Buda, C.; Neurock, M.; Iglesia, E. Chemisorption of CO and Mechanism of CO Oxidation on Supported Platinum Nanoclusters. *J. Am. Chem. Soc.* **2011**, *133* (12), 4498−4517.
(33) Wang, L.; Yi, Y.; Guo, H.; Tu, X. Atmospheric Pressure and Room Temperature Synthesis of Methanol through Plasma-Catalytic Hydrogenation of CO_2. *ACS Catal.* **2018**, *8* (1), 90−100.
(34) Xu, S.; Chansai, S.; Stere, C.; Inceesungvorn, B.; Goguet, A.; Wangkawong, K.; Taylor, S. F. R.; Al-Janabi, N.; Hardacre, C.; Martin, P. A.; Fan, X. Sustaining Metal-Organic Frameworks for Water-Gas Shift Catalysis by Non-Thermal Plasma. *Nat. Catal.* **2019**, *2* (2), 142−148.
(35) Zhao, J.; Liu, J.; Li, Z.; Wang, K.; Shi, R.; Wang, P.; Wang, Q.; Waterhouse, G. I. N.; Wen, X.; Zhang, T. Ruthenium-Cobalt Single Atom Alloy for CO Photo-Hydrogenation to Liquid Fuels at Ambient Pressures. *Nat. Commun.* **2023**, *14* (1), 1909.
(36) Redhead, P. A. Thermal Desorption of Gases. *Vacuum* **1962**, *12* (4), 203−211.
(37) Zakem, G.; Christopher, P. Active Site Entropy of Atomically Dispersed Rh/Al2O3 Catalysts Dictates Activity for Ethylene Hydroformylation. *ACS Catal.* **2023**, *13* (8), 5502−5515.
(38) Godyak, V. A.; Piejak, R. B. In situ Simultaneous Radio Frequency Discharge Power Measurements. *J. Vac. Sci. Technol., A* **1990**, *8* (5), 3833−3837.
(39) Herz, R. K.; Kiela, J. B.; Marin, S. P. Adsorption Effects during Temperature-Programmed Desorption of Carbon Monoxide from Supported Platinum. *J. Catal.* **1982**, *73* (1), 66−75.
(40) Qi, J.; Resasco, J.; Robatjazi, H.; Alvarez, I. B.; Abdelrahman, O.; Dauenhauer, P.; Christopher, P. Dynamic Control of Elementary Step Energetics via Pulsed Illumination Enhances Photocatalysis on Metal Nanoparticles. *ACS Energy Lett.* **2020**, *5* (11), 3518−3525.
(41) Golibrzuch, K.; Shirhatti, P. R.; Geweke, J.; Werdecker, J.; Kandratsenka, A.; Auerbach, D. J.; Wodtke, A. M.; Bartels, C. CO Desorption from a Catalytic Surface: Elucidation of the Role of Steps by Velocity-Selected Residence Time Measurements. *J. Am. Chem. Soc.* **2015**, *137* (4), 1465−1475.
(42) Ertl, G.; Neumann, M.; Streit, K. M. Chemisorption of CO on the Pt(111) surface. *Surf. Sci.* **1977**, *64* (2), 393−410.
(43) Cao, S.; Tao, F. F.; Tang, Y.; Li, Y.; Yu, J. Size- and Shape-Dependent Catalytic Performances of Oxidation and Reduction Reactions on Nanocatalysts. *Chem. Soc. Rev.* **2016**, *45*, 4747−4765.
(44) Falbo, L.; Visconti, C. G.; Lietti, L.; Szanyi, J. The Effect of CO on CO_2 Methanation over Ru/Al_2O_3 Catalysts: A Combined Steady-State Reactivity and Transient DRIFT Spectroscopy Study. *Appl. Catal., B* **2019**, *256*, 117791.
(45) Berrospe-Rodriguez, C.; Schwan, J.; Nava, G.; Kargar, F.; Balandin, A. A.; Mangolini, L. Interaction between a Low-Temper-

https://doi.org/10.1021/jacsau.4c00309
JACS Au 2024, 4, 2979−2988

ature Plasma and Graphene: An in Situ Raman Thermometry Study. *Phys. Rev. Appl.* **2021**, *15* (2), 024018.
(46) Yadava, N.; Chauhan, R. K.; Allen, J. E. An Electrostatic Probe Technique for RF Plasma. *J. Phys. E: Sci. Instrum.* **1987**, *20*, 1046−1049.
(47) Kim, M.; Mangolini, L. Using Surface-Enhanced Raman Spectroscopy to Probe Surface-Localized Nonthermal Plasma Activation. *J. Phys. Chem. Lett.* **2024**, *15* (15), 4136−4141.
(48) Steininger, H.; Lehwald, S.; Ibach, H. On the adsorption of CO on Pt(111). *Surf. Sci.* **1982**, *123* (2−3), 264−282.
(49) Fair, J.; Madix, R. J. Low and High Coverage Determinations of the Rate of Carbon Monoxide Adsorption and Desorption from Pt(110). *J. Chem. Phys.* **1980**, *73* (7), 3480−3485.
(50) Shan, B.; Zhao, Y.; Hyun, J.; Kapur, N.; Nicholas, J. B.; Cho, K. Coverage-Dependent CO Adsorption Energy from First-Principles Calculations. *J. Phys. Chem. C* **2009**, *113* (15), 6088−6092.
(51) Kale, M. J.; Avanesian, T.; Xin, H.; Yan, J.; Christopher, P. Controlling Catalytic Selectivity on Metal Nanoparticles by Direct Photoexcitation of Adsorbate-Metal Bonds. *Nano Lett.* **2014**, *14* (9), 5405−5412.
(52) Barraza Alvarez, I.; Le, T.; Hosseini, H.; Samira, S.; Beck, A.; Marlowe, J.; Montemore, M. M.; Wang, B.; Christopher, P. Bond Selective Photochemistry at Metal Nanoparticle Surfaces: CO Desorption from Pt and Pd. *J. Am. Chem. Soc.* **2024**, *146* (18), 12431−12443.
(53) Sangnier, A.; Genty, E.; Iachella, M.; Sautet, P.; Raybaud, P.; Matrat, M.; Dujardin, C.; Chizallet, C. Thermokinetic and Spectroscopic Mapping of Carbon Monoxide Adsorption on Highly Dispersed Pt/γ-Al2O3. *ACS Catal.* **2021**, *11* (21), 13280−13293.
(54) Collins, D. M.; Spicer, W. E. The adsorption of CO, O_2, and H_2 on Pt: I. Thermal desorption spectroscopy studies. *Surf. Sci.* **1977**, *69* (1), 85−113.
(55) Mcclellan, M. R.; Gland, J. L.; Mcfeeley, F. R. Carbon monoxide adsorption on the kinked Pt(321) surface. *Surf. Sci.* **1981**, *112* (1−2), 63−77.
(56) Kalff, M.; Comsa, G.; Michely, T. How Sensitive Is Epitaxial Growth to Adsorbates? *Phys. Rev. Lett.* **1998**, *81* (6), 1255−1258.
(57) Bal, K. M.; Huygh, S.; Bogaerts, A.; Neyts, E. C. Effect of Plasma-Induced Surface Charging on Catalytic Processes: Application to CO_2 Activation. *Plasma Sources Sci. Technol.* **2018**, *27* (2), 024001.
(58) Jafarzadeh, A.; Bal, K. M.; Bogaerts, A.; Neyts, E. C. Activation of CO_2 on Copper Surfaces: The Synergy between Electric Field, Surface Morphology, and Excess Electrons. *J. Phys. Chem. C* **2020**, *124* (12), 6747−6755.
(59) Chen, S.; Wang, Y.; Li, Q.; Li, K.; Li, M.; Wang, F. A DFT Study of Plasma-Catalytic Ammonia Synthesis: The Effect of Electric Fields, Excess Electrons and Catalyst Surfaces on N_2 Dissociation. *Phys. Chem. Chem. Phys.* **2023**, *25* (5), 3920−3929.
(60) Onn, T. M.; Gathmann, S. R.; Guo, S.; Solanki, S. P. S.; Walton, A.; Page, B. J.; Rojas, G.; Neurock, M.; Grabow, L. C.; Mkhoyan, K. A.; Abdelrahman, O. A.; Frisbie, C. D.; Dauenhauer, P. J. Platinum Graphene Catalytic Condenser for Millisecond Programmable Metal Surfaces. *J. Am. Chem. Soc.* **2022**, *144* (48), 22113−22127.
(61) Hutter, J.; Iannuzzi, M.; Schiffmann, F.; Vandevondele, J. Cp2k: Atomistic Simulations of Condensed Matter Systems. *Wiley Interdiscip. Rev. Comput. Mol. Sci.* **2014**, *4* (1), 15−25.
(62) Kühne, T. D.; Iannuzzi, M.; Del Ben, M.; Rybkin, V. V.; Seewald, P.; Stein, F.; Laino, T.; Khaliullin, R. Z.; Schütt, O.; Schiffmann, F.; et al. CP2K: An Electronic Structure and Molecular Dynamics Software Package - Quickstep: Efficient and Accurate Electronic Structure Calculations. *J. Chem. Phys.* **2020**, *152*, 194103.
(63) Bal, K. M.; Neyts, E. C. Modelling Molecular Adsorption on Charged or Polarized Surfaces: A Critical Flaw in Common Approaches. *Phys. Chem. Chem. Phys.* **2018**, *20* (13), 8456−8459.
(64) Jafarzadeh, A.; Bal, K. M.; Bogaerts, A.; Neyts, E. C. CO_2 Activation on TiO_2-Supported Cu_5 and Ni_5 Nanoclusters: Effect of Plasma-Induced Surface Charging. *J. Phys. Chem. C* **2019**, *123* (11), 6516−6525.
(65) Lee, H. J.; Ho, W. Single-Bond Formation and Characterization with a Scanning Tunneling Microscope. *Science* **1999**, *286* (5445), 1719−1722.
(66) Lee, J.; Sorescu, D. C.; Deng, X. Electron-Induced Dissociation of CO_2 on TiO_2(110). *J. Am. Chem. Soc.* **2011**, *133* (26), 10066−10069.
(67) Sode, M.; Jacob, W.; Schwarz-Selinger, T.; Kersten, H. Measurement and Modeling of Neutral, Radical, and Ion Densities in H_2-N_2-Ar Plasmas. *J. Appl. Phys.* **2015**, *117* (8), 083303.
(68) Lippert, G.; Hutter, J.; Parrinello, M. A Hybrid Gaussian and Plane Wave Density Functional Scheme. *Mol. Phys.* **1997**, *92* (3), 477−487.
(69) Goedecker, S.; Teter, M.; Hutter, J. Separable Dual-Space Gaussian Pseudopotentials. *Phys. Rev.* **1996**, *54* (3), 1703−1710.
(70) Hartwigsen, C.; Goedecker, S.; Hutter, J. Relativistic Separable Dual-Space Gaussian Pseudopotentials from H to Rn. *Phys. Rev.* **1998**, *58* (7), 3641−3662.
(71) Perdew, J. P.; Burke, K.; Ernzerhof, M. Generalized Gradient Approximation Made Simple. *Phys. Rev. Lett.* **1996**, *77* (18), 3865−3868.
(72) Smith, D. G. A.; Burns, L. A.; Patkowski, K.; Sherrill, C. D. Revised Damping Parameters for the D3 Dispersion Correction to Density Functional Theory. *J. Phys. Chem. Lett.* **2016**, *7* (12), 2197−2203.
(73) Hub, J. S.; De Groot, B. L.; Grubmüller, H.; Groenhof, G. Quantifying Artifacts in Ewald Simulations of Inhomogeneous Systems with a Net Charge. *J. Chem. Theory Comput.* **2014**, *10* (1), 381−390.
(74) Martyna, G. J.; Tuckerman, M. E. A Reciprocal Space Based Method for Treating Long Range Interactions in Ab Initio and Force-Field-Based Calculations in Clusters. *J. Chem. Phys.* **1999**, *110* (6), 2810−2821.

https://doi.org/10.1021/jacsau.4c00309
JACS Au 2024, 4, 2979−2988